

See discussions, stats, and author profiles for this publication at: <https://www.researchgate.net/publication/231682866>

# Electron diffraction study on the two crystalline phases occurring in native cellulose from an algal cell wall. Macromolecules

ARTICLE *in* MACROMOLECULES · JULY 1991

Impact Factor: 5.8 · DOI: 10.1021/ma00014a033

---

CITATIONS

467

READS

45

---

## 3 AUTHORS, INCLUDING:



[Junji Sugiyama](#)

Kyoto University

209 PUBLICATIONS 7,059 CITATIONS

[SEE PROFILE](#)



[Henri Chanzy](#)

French National Centre for Scientific Res...

69 PUBLICATIONS 4,798 CITATIONS

[SEE PROFILE](#)

# Electron Diffraction Study on the Two Crystalline Phases Occurring in Native Cellulose from an Algal Cell Wall

Junji Sugiyama,<sup>†</sup> Roger Vuong, and Henri Chanzy\*

*Centre de Recherches sur les Macromolécules Végétales, CNRS,<sup>‡</sup> B.P. 53X,  
38041 Grenoble Cedex, France*

*Received November 21, 1990; Revised Manuscript Received February 12, 1991*

**ABSTRACT:** Cellulose from the cell wall of the green alga *Microdictyon tenuius* was studied by electron diffraction. The diffractograms disclose two distinct crystalline phases. The major phase has a one-chain, triclinic ( $P\bar{1}$ ) structure with unit cell parameters of  $a = 0.674$  nm,  $b = 0.593$  nm,  $c$  (chain axis) = 1.036 nm,  $\alpha = 117^\circ$ ,  $\beta = 113^\circ$ , and  $\gamma = 81^\circ$ . The crystal unit cell of the minor component has two chains and is monoclinic ( $P2_1$ ), with  $a = 0.801$  nm,  $b = 0.817$  nm,  $c$  (chain axis) = 1.036 nm, and  $\gamma$  the monoclinic angle =  $97.3^\circ$ . The triclinic phase is metastable, and annealing it in dilute alkali at  $260^\circ\text{C}$  converts it into the monoclinic form. The presence of two phases in *Microdictyon* can be extended to other algal celluloses and is consistent with the biphasic character deduced from  $^{13}\text{C}$  CP/MAS NMR spectroscopy. The triclinic and the monoclinic structures correspond to the I $\alpha$  and I $\beta$  spectra, respectively.

## Introduction

More than 60 years have passed since the general features of native crystalline cellulose were outlined by Meyer and Mark.<sup>1</sup> Since the work of these pioneers, the resolution of the three-dimensional structure of crystalline cellulose has been the focus of a number of investigations.<sup>2–8</sup> So far, these studies have failed to produce a unified model that would describe unambiguously the molecular arrangement of cellulose within its crystal. In terms of diffraction analysis, native cellulose yields different patterns, depending on its origin. On the one hand, algal cellulose such that as found in the cell wall of *Valonia* or *Chaetomorpha*<sup>9–11</sup> gives well-resolved diffraction diagrams that require an 8-chain unit cell and a  $P\bar{1}$  space group to be properly indexed as a one-phase component. On the other hand, celluloses from higher plants give diffraction patterns that can be indexed according to a smaller unit cell: typically, a ramie cellulose diagram corresponds to a two-chain unit cell with a symmetry that can be approximated to  $P2_1$ .<sup>5–8</sup>

Very recently, Sugiyama et al.<sup>12</sup> have examined new diffraction diagrams of *Valonia* cellulose. According to their observations, *Valonia* cellulose appears to be composed of two crystalline phases: a monoclinic two-chain component that resembles closely ramie cellulose and also a triclinic component whose unit cell could not be established with certainty. A great advantage of the two-phase model for crystalline *Valonia* cellulose is that it explains quite nicely the fine details of the high-resolution solid-state  $^{13}\text{C}$  CP/MAS NMR spectra recorded for such specimens. In these spectra, a peak multiplicity is found for each carbon atom. The origin of such spectral multiplicity was well explained by Atalla and Vander-Hart,<sup>13–16</sup> who showed by this technique that two phases, namely, cellulose I $\alpha$  and cellulose I $\beta$  coexisted in several native celluloses. According to these authors, the proportion I $\alpha$ /I $\beta$  was estimated at 65%/35% for *Valonia* cellulose.<sup>14</sup> This proportion varied greatly when samples other than algal cellulose were considered. More recently, also with  $^{13}\text{C}$  CP/MAS spectroscopy, Horii et al. showed that the I $\alpha$  phase of cellulose was metastable and could

be converted readily into the thermodynamically stable I $\beta$  phase following a hydrothermal annealing treatment.<sup>16,17</sup> By analysis of the  $^{13}\text{C}$  CP/MAS spectra of *Valonia* cellulose before and after annealing and correlation of these spectra with the corresponding diffraction patterns, it became clear that the monoclinic phase of cellulose could be identified as the I $\beta$  phase whereas the triclinic phase corresponded to the I $\alpha$ .<sup>12</sup>

There are a number of questions that need to be answered concerning the identification and coexistence of the two crystalline phases of native cellulose in *Valonia*. In particular, the exact size and localization of the domains corresponding to the two phases have to be determined if one wants to attempt the recording of diffraction diagrams of each phase.

In a recent report we have shown that the two crystalline phases of cellulose could also be observed by Fourier transform infrared (FT-IR) spectroscopy.<sup>18</sup> In particular, there were two infrared bands specific to the I $\alpha$  phase that could be identified in unannealed cellulose samples of either bacterial or algal origin. In one of these algae, *Microdictyon tenuius*, these two cellulose bands appeared to be narrower and better resolved than in most other specimens such as *Valonia*, *Glauccystis*, *Rhizoclonium*, etc. Thus, *Microdictyon* cellulose appeared to contain well-defined highly crystalline domains of the I $\alpha$  phase. This observation prompted us to prepare batches of microcrystals of *Microdictyon* and to subject some of them to an annealing treatment. The goal of these experiments was to record a set of electron diffractograms specific of the pure I $\alpha$  (with unannealed samples) and pure I $\beta$  (with the annealed samples) phases. The presentation of these diagrams together with their significance for the understanding of the structure of cellulose is described here.

## Experimental Section

**Materials.** *Microdictyon* is a green marine alga from the order of *Siphonocladiales* whose structure is based on strings of cells having around 0.5 mm in length and from 0.2 to 0.5 mm in width. Branching occurs every second or third cells, and there may be one or two branches on a given cell. The samples used in this study (a kind gift from the late B. Caram) were collected in the Bay of Villefranche near Nice, France. After harvesting, the samples were kept suspended in ethanol until their treatment described below.

**Sample Preparation. Ultrathin Sections of the Cell Wall.** The cell walls of *Microdictyon* were purified by boiling in 0.1 N

\* To whom all correspondence should be addressed.

<sup>†</sup> Permanent address: Department of Forest Products, Faculty of Agriculture, The University of Tokyo, Bunkyo-ku, Tokyo 113, Japan.

<sup>‡</sup> Affiliated with the Joseph Fourier University of Grenoble.

NaOH for 10 h followed by rinsing overnight in 0.05 N HCl with gentle stirring. The cell walls were then dehydrated and embedded in epoxy resin following standard procedure. Ultrathin sections about 50 nm thick were cut with an LKB microtome (Ultratome 4) after positioning a block in such a way that the longer axis of the embedded cells (i.e., a filament direction) was perpendicular to the cutting direction. Under such conditions, the cutting was achieved perpendicular to one of the two major microfibril orientations.

**Microcrystals of the I $\alpha$  and I $\beta$  Phases.** Samples purified in the same manner as above were hydrolyzed by boiling in 2.5 N HCl for 4 h. The resulting microcrystals, which consisted almost essentially of the I $\alpha$  phase, were neutralized and washed by repeating centrifugation in water. They were then stored in water, to which a drop of chloroform was added in order to avoid bacterial contamination.

For the preparation of microcrystals of the I $\beta$  phase, a portion of the above microcrystals was subjected to a hydrothermal treatment.<sup>17</sup> For this, a suspension of the crystals in 0.1 N NaOH was poured into an autoclave whose temperature was brought to 260 °C by immersion in an oil bath. This temperature was maintained for 45 min, after which the autoclave was quenched under tap water. The crystals were then recovered and their conversion to I $\beta$  was monitored by FT-IR spectroscopy with the help of a Perkin-Elmer 1720X instrument: the disappearance of two specific absorption bands of the I $\alpha$  phase (3240 and 750 cm<sup>-1</sup>)<sup>18</sup> indicated the total conversion into the I $\beta$  phase.

**Electron Microscopy.** All electron micrographs and electron diffraction patterns were recorded with a Philips EM 400T operated at an accelerating voltage of 120 kV. The images and diffraction diagrams were recorded on Mitsubishi electron microscopic films (MEM), which were developed in an Ilford PQ universal developer (diluted with water: 150/1850 v/v) from 5 to 7 min at 20 °C.

The recording of microdiffraction diagrams from a single microcrystal or microfibril was successfully achieved by using the diffraction method of Riecke.<sup>19,20</sup> For this, a 5-μm aperture was inserted in the C2 condenser lens while the C1 condenser was overfocused to its maximum. Under such conditions, diffraction patterns with a high angular resolution could be obtained from specimen areas having a diameter as small as 20–100 nm while the remainder of the sample was kept unirradiated. For recording the diffraction patterns and in order to avoid specimen damage prior to photographing, all adjustments were achieved with an extremely weak electron beam current. With such a low illumination, the diffraction patterns could be selected and adjusted only with the help of a Lhesa image intensifier.

For recording diffraction contrast images in both bright and dark fields, a small objective aperture (10 or 20 μm) was used to select either the transmitted beam or one of the diffracted beams from the crystals. Bright-field images were recorded at a plate magnification of 17 000–22 000 $\times$ , whereas dark-field images were obtained at a magnification ranging from 2800 $\times$  to 4600 $\times$ .

**Unit Cell Refinement.** From a large number of electron diffractograms that were recorded, only those containing the information of one phase were considered. These diagrams were calibrated with a gold standard, and the interplanar distances corresponding to each spot were calculated. After proper indexing, the unit cells of the two phases were refined by using a least-squares refinement program (SALS: statistical analysis with least square fitting, a library program from the University of Tokyo).

## Results

The purified cell walls of *Microdictyon* can be delaminated to yield layers of parallel cellulose microfibrils suitable for electron microscopy and electron diffraction analysis. In Figure 1A, a portion of such a layer is shown. It consists of a bundle of well-oriented cellulose and apparently endless microfibrils. When the cross section of such bundles are observed by diffraction contrast electron microscopy, each microfibril section is seen as a squarish small black area about 25–35 nm wide. The microfibrils of *Microdictyon* are thus substantially larger than those of most celluloses, even those of *Valonia*.<sup>21</sup>

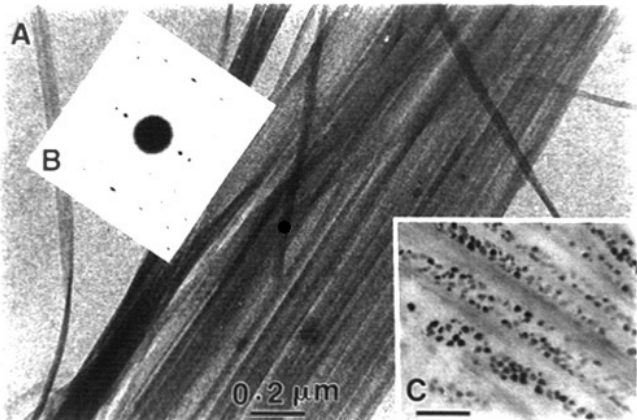


**Figure 1.** Ultrastructural features of *Microdictyon* cellulose microfibrils: (A) a thin layer of microfibrils unstained and unshadowed observed under low-dose imaging conditions; (B) bright-field electron micrograph of the cross section of a cell wall fragment of *Microdictyon* (the almost square section of the microfibrils is well denoted in this diffraction contrast image); (C) electron diffraction diagram of an area such as that located in the lower part of Figure 1A and recorded on an area having 200 nm in diameter.

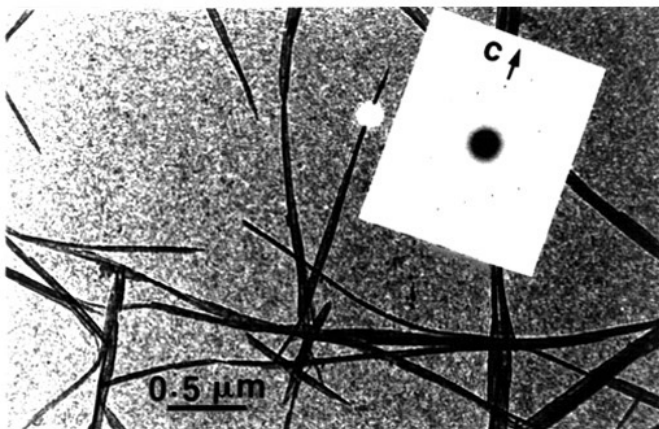
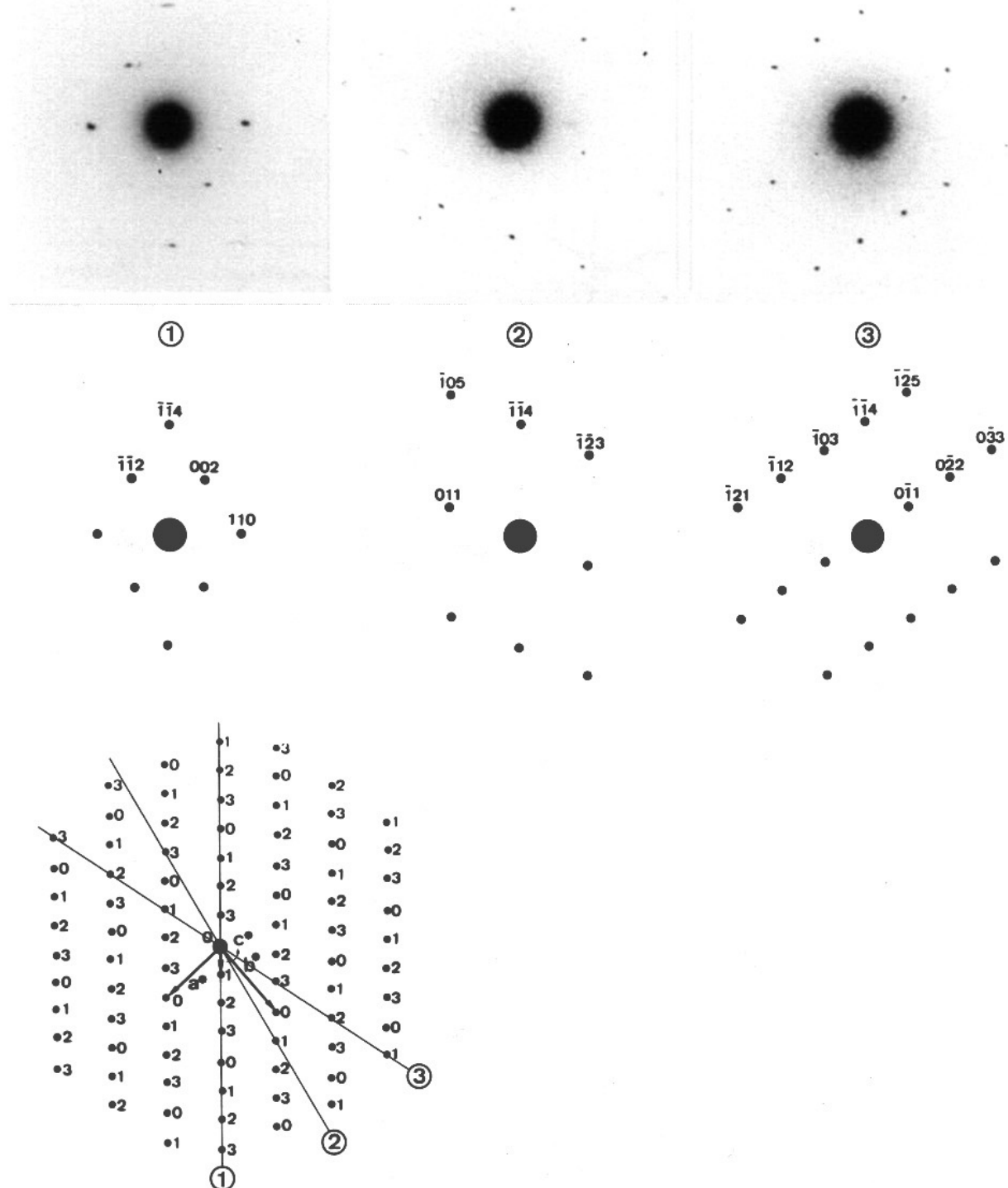


**Figure 2.** Electron micrograph of cellulose microcrystals obtained after acid hydrolysis of *Microdictyon* cellulose. Inset: typical triclinic spot pattern recorded on an area of the specimen such as outlined in white in the corresponding micrograph. The direction *c* is the cellulose chain axis, which is aligned with the microcrystal long axis. The diagram is properly oriented with respect to the picture.

The perfection of the orientation of the microfibrils of *Microdictyon* is confirmed by the electron diffraction diagram (Figure 1C) recorded on an area of the specimen having a diameter of around 200 nm. Despite a substantial biaxial orientation denoted by the weakness of the equatorial diffraction spot at 0.620 nm, this pattern contains all the characteristics of a fiber pattern. In Figure 1C, the diffraction spots are strikingly devoid of any arcing. This indicates that in the area selected for the electron diffraction (lower half of Figure 1A) the crystals of cellulose have their chain axes in rigorous alignment along the microfibril direction. Another feature of the diagram in Figure 1C is that it presents the characteristics of a triclinic fiber diagram. This is clearly seen in the first, third, and fifth layer lines where some of the spots in the left part of the diagram are not mirrored in the right.

During acid hydrolysis, the cellulose microfibrils of *Microdictyon* cellulose break down into microcrystalline elements commonly called "cellulose microcrystals". They have the same width (25–35 nm) as the initial microfibrils but lengths ranging from 1 to 10 μm only. In terms of crystallinity and crystal quality, these microcrystals have the same perfection as the initial microfibrils: this is denoted by their FT-IR spectrum, which is undistinguish-

A

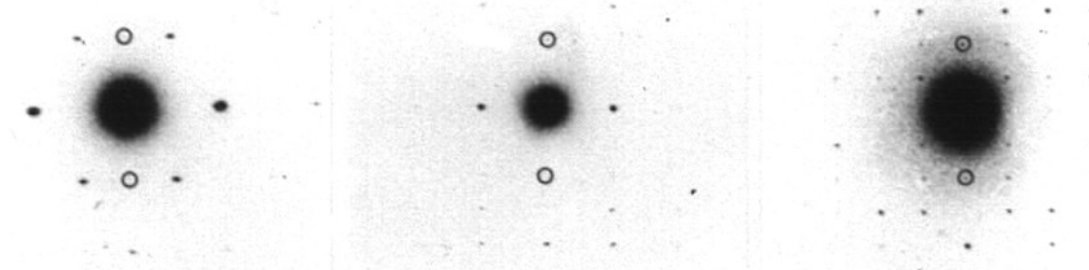
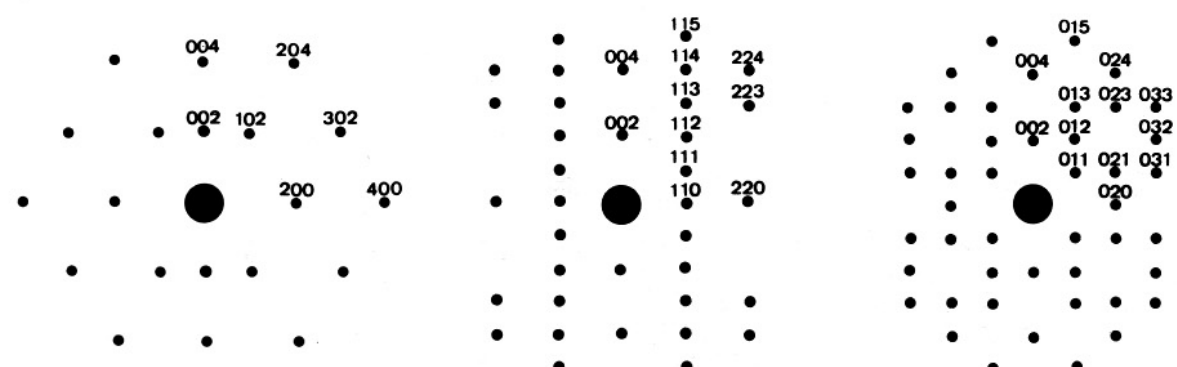
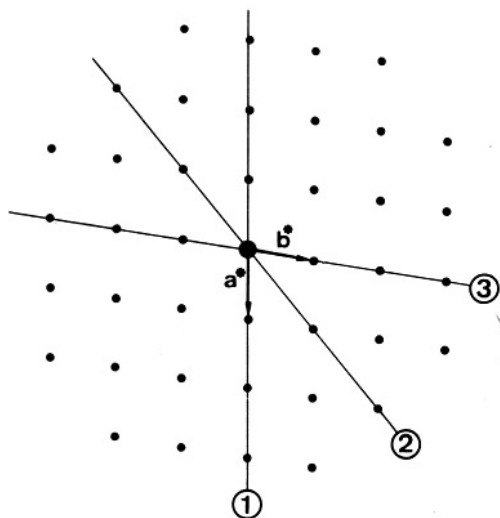


**Figure 3.** (A) A series of spot electron diffractograms presenting the triclinic features and recorded as in Figure 2. (B) Corresponding indexations. (C) Projection of the reciprocal lattice perpendicular to the chain direction *c*. The spots with number zero indicate reciprocal lattice points located on the layer lines indexed with  $4n$  ( $n = 0, 1, 2, \dots$ ). The spots with numbers 1–3 correspond to reciprocal lattice points located on the layer lines indexed with  $4n + 1, 4n + 2, 4n + 3$ , respectively. The lines marked circled 1–3 correspond to the traces of the sections that are presented in Figures 3A (circled 1–3).

able from the initial desincrustated *Microdictyon*. A preparation of these microcrystals is shown in Figure 2. Each microcrystal can be scanned in diffraction mode by using the Riecke method,<sup>19,20</sup> which is well adapted to obtain a diffraction pattern on specimen areas with dimensions of 50 nm or even smaller. When applied to the *Microdictyon* microcrystals, this technique yields single-crystal diagrams such as the one inserted in Figure 2. In this diffractogram, the diffraction spots are aligned in layer lines that make an angle markedly different from 90° with respect to the cellulose chain direction, which coincides with the microcrystal long axis. A diagram such

as the one in Figure 2 contains, in particular, some of the spots that were identified as triclinic in the fiber diffraction diagram of *Microdictyon* cellulose. Therefore, this diagram corresponds to a section of the reciprocal lattice of the triclinic phase of cellulose, the space group of which must be *P*1. (The other triclinic space group, *P*1̄, is centrosymmetric and is not compatible with structures that contain only D-glucose.)

Numerous other single-crystal diffraction diagrams were recorded, both before and after applying the annealing treatment. Figure 3 and related patterns could only be recorded from samples that had not been annealed. These

**A****B****C**

**Figure 4.** (A) A series of spot electron diffractograms obtained on annealed *Microdictyon* and presenting the monoclinic character. (B) Corresponding indexation. (C) Cross section of the reciprocal lattice perpendicular to the chain direction  $c$  (coincident with  $c^*$  in monoclinic mode). The lines marked circled 1-3 correspond to the traces of the sections that are presented in Figures 4A (circled 1-3).

patterns have rows of diffraction spots that are inclined with respect to the crystal axes and thus correspond to the triclinic phase. Figure 4 shows the monoclinic diffraction pattern that occurs less commonly in the unannealed material but is the only pattern found in annealed samples. The patterns in Figure 4 all have orthogonal symmetry, with layer lines perpendicular to the microcrystal axis. These patterns correspond to a monoclinic phase, and  $c$  is the unique axis. Since only even-ordered reflections are present along this axis, the space group of the corresponding phase must be  $P2_1$ .

The list of the reflections that were measured and indexed in each family are presented in Tables I (triclinic) and II (monoclinic). In Table I, there are 27 independent

reflections. All of them can be indexed using a one-chain  $P1$  triclinic unit cell with dimensions  $a = 0.674 \text{ nm}$ ,  $b = 0.593 \text{ nm}$ ,  $c$  (chain axis) =  $1.036 \text{ nm}$ ,  $\alpha = 117^\circ$ ,  $\beta = 113^\circ$ ,  $\gamma = 81^\circ$ , cell volume =  $0.3395 \text{ nm}^3$ , and calculated density = 1.582.

In Table II, the list contains 38 independent diffraction spots. All the spots can be indexed along a two-chain  $P2_1$  unit cell with dimensions  $a = 0.801 \text{ nm}$ ,  $b = 0.817 \text{ nm}$ ,  $c$  (chain axis and unique monoclinic axis) =  $1.036 \text{ nm}$ ,  $\alpha = \beta = 90^\circ$ ,  $\gamma = 97.3^\circ$ , cell volume =  $0.6725 \text{ nm}^3$ , and calculated density = 1.599.

In the light of these observations, the fiber diffraction diagram of *Microdictyon* cellulose can be fully indexed as being a superposition of a one-chain triclinic fiber dif-

**Table I**  
Observed and Calculated  $d$ -Spacings Corresponding to the Triclinic Crystalline Phase of Cellulose

indices			$d_{\text{obs}}$ , nm	$d_{\text{calc}}$ , nm	$d_{\text{obs}} - d_{\text{calc}}$ , nm
$h$	$k$	$l$	Zero Layer Line		
1	0	0	0.620	0.621	-0.001
0	1	0	0.531	0.528	0.003
1	1	0	0.396	0.397	-0.001
2	2	0	0.198	0.198	0.000
First Layer Line			Zero Layer Line		
0	-1	1 <sup>a</sup>	0.574	0.575	-0.001
0	1	1	0.381	0.382	-0.001
-1	2	1 <sup>a</sup>	0.223	0.221	0.002
-3	0	1	0.219	0.220	-0.001
Second Layer Line			First Layer Line		
-1	-1	2	0.439	0.438	0.001
0	0	2	0.432	0.430	0.002
0	-2	2	0.286	0.287	-0.001
-1	1	2	0.281	0.282	-0.001
-2	-2	2	0.235	0.238	-0.003
1	1	2	0.233	0.234	-0.001
Third Layer Line			Second Layer Line		
-1	0	3 <sup>a</sup>	0.306	0.306	0.000
-1	-2	3 <sup>a</sup>	0.269	0.268	0.001
1	-1	3	0.246	0.246	0.000
-1	1	3	0.222	0.224	-0.002
0	-3	3 <sup>a</sup>	0.191	0.191	0.000
Fourth Layer Line			Third Layer Line		
-1	-1	4	0.259	0.259	0.000
-1	-2	4	0.235	0.235	0.000
-1	0	4	0.231	0.230	0.001
-2	-2	4	0.220	0.219	0.001
0	0	4	0.216	0.215	0.001
-1	-3	4	0.188	0.187	0.001
Fifth Layer Line			Fourth Layer Line		
-1	-2	5	0.198	0.199	-0.001
-1	0	5 <sup>a</sup>	0.183	0.184	-0.001

<sup>a</sup> Triclinic spots that are clearly identified in the fiber diffraction diagram of the initial sample.

fraction diagram on a two-chain monoclinic fiber pattern. In the monoclinic as well as in the triclinic diagrams, the layer lines are coincident. This is because both crystalline phases share the same chain axis direction and have the same  $c$  parameter of 1.036 nm. A diagram such as the one shown in Figure 1C is a superposition of two diffraction patterns, and there are a number of reflections that overlap one another. This occurs, in particular, on the equator, the second and fourth layer lines. With the help of the diffractograms of each phase, such as those shown on Figures 3 and 4, the deconvolution of the pattern in Figure 1C becomes possible. For instance, on the equator, the three strong diffraction spots of cellulose are present in both diagrams: the innermost reflection is observed at  $d = 0.620$  nm in the triclinic case but at  $d = 0.612$  nm in the monoclinic diagram. The second innermost reflection is at 0.531 nm in the triclinic crystal versus 0.536 nm in the monoclinic. Finally, the reflection at 0.396 nm is coincident in the diagrams of both phases. On the first, third, and fifth layer lines, there are several isolated triclinic spots: the fairly strong diffraction spots at 0.306 and 0.269 nm in the third layer line are not overlapped by any monoclinic diffraction spots. These two spots can be used to verify the presence of a triclinic phase in any given sample. In the monoclinic diagram, the meridional spot at 0.518 nm and indexed as 002 is not found in any of the triclinic diffraction diagrams: its presence indicates that the specimen contains some monoclinic phase. As the meridional 004 diffraction spot (indexed as  $\bar{1}\bar{1}4$  in the triclinic diagram) is common to both phases, one can calculate the proportion of monoclinic and triclinic phases by

**Table II**  
Observed and Calculated  $d$ -Spacings Corresponding to the Monoclinic Phase of Cellulose

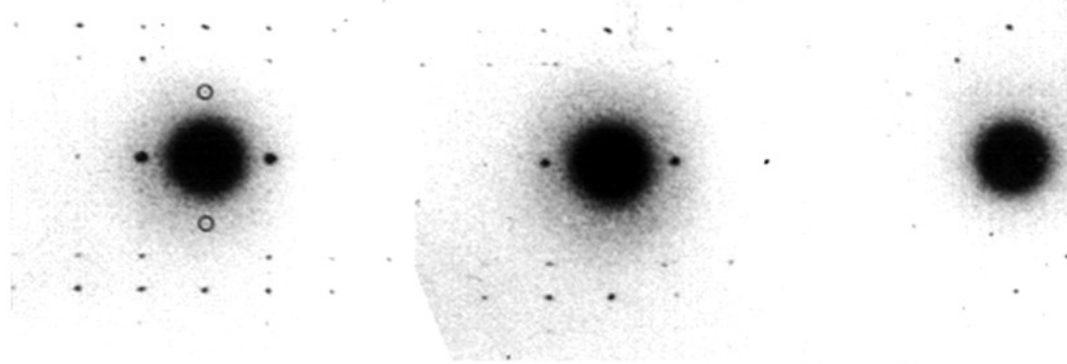
indices			$d_{\text{obs}}$ , nm	$d_{\text{calc}}$ , nm	$d_{\text{obs}} - d_{\text{calc}}$ , nm
$h$	$k$	$l$	Zero Layer Line		
1	-1	0	0.612	0.607	0.005
1	1	0	0.536	0.535	0.001
2	0	0	0.396	0.397	-0.001
2	1	0	0.344	0.339	0.005
2	2	0	0.266	0.267	-0.001
0	4	0	0.205	0.203	0.002
First Layer Line			First Layer Line		
0	1	1	0.636	0.638	-0.002
1	1	1	0.476	0.475	0.001
0	2	1	0.378	0.377	0.001
2	1	1	0.324	0.323	0.001
0	3	1	0.262	0.261	0.001
-2	3	1	0.227	0.232	-0.005
0	4	1	0.200	0.199	0.001
Second Layer Line			Second Layer Line		
0	0	2 <sup>a</sup>	0.518	0.518	0.000
0	1	2	0.435	0.436	-0.001
1	0	2	0.430	0.434	-0.004
1	1	2	0.371	0.372	-0.001
-1	2	2	0.303	0.307	-0.003
1	2	2	0.287	0.286	0.001
0	3	2	0.239	0.240	-0.001
-2	3	2	0.213	0.216	-0.003
Third Layer Line			Third Layer Line		
0	1	3	0.316	0.318	-0.002
1	-1	3	0.299	0.300	-0.001
1	1	3	0.289	0.290	-0.001
0	2	3	0.262	0.263	-0.001
1	2	3	0.245	0.244	0.001
0	3	3	0.213	0.213	0.000
Fourth Layer Line			Fourth Layer Line		
0	0	4	0.259	0.259	0.000
1	1	4	0.232	0.233	-0.001
0	2	4	0.218	0.218	0.000
2	2	4	0.186	0.186	0.000
4	2	4	0.142	0.142	0.000
Fifth Layer Line			Fifth Layer Line		
0	1	5	0.201	0.201	0.000
1	1	5	0.196	0.193	0.003
2	1	5	0.179	0.177	0.002
2	3	5	0.149	0.148	0.001

<sup>a</sup> This spot, which is not present in the triclinic diagram, is a clear identification of the monoclinic phase in the fiber diffraction diagram of the initial sample.

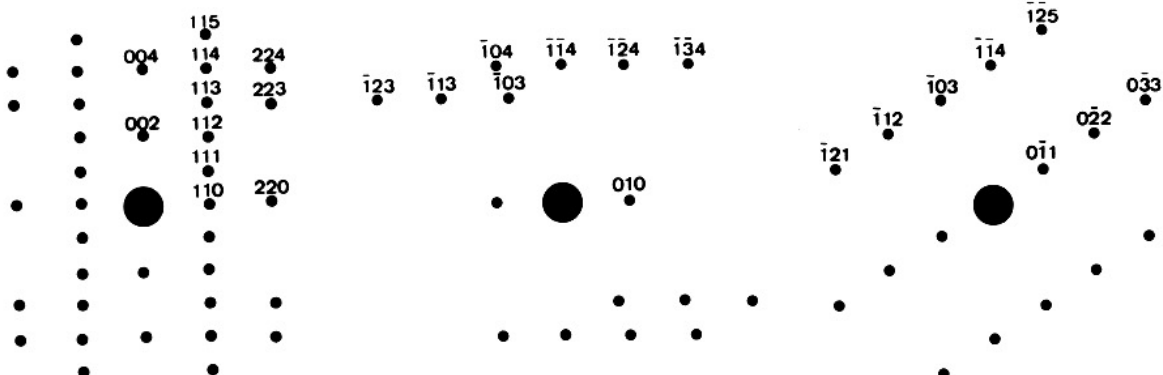
measuring the ratio of the intensities,  $I_{002}/I_{004}$ , in a given sample and comparing it with the same ratio measured in an annealed sample.

In the initial unannealed sample, both monoclinic and triclinic patterns can be recorded during sequential examination of a single particle. Therefore a "micro-crystal" consists of contiguous crystalline blocks corresponding to either one or the other phase. This is demonstrated by the sequence shown in Figure 5 where the three diffractograms were recorded at distances separated by about 50 nm. In Figure 5A (circled 1), a monoclinic diagram identical with that shown in Figure 4A (circled 2) was observed. Fifty nanometers further along the same microcrystal, a pattern that contains both monoclinic and triclinic information was recorded [Figure 5A (circled 2)]. Still further along the same microcrystal, a pure triclinic pattern [Figure 5A (circled 3)] was obtained again. Thus, along one microcrystal, the monoclinic and the triclinic phases are successfully found in domains large enough to give well-resolved electron diffractograms. The

A



B



C

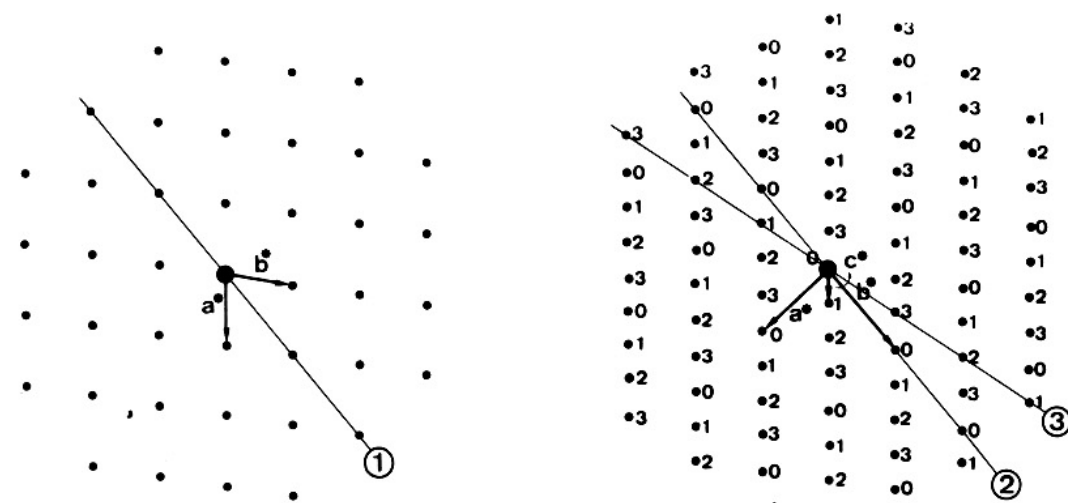


**Figure 5.** (A) A series of spot electron diffractograms recorded sequentially at 50-nm distance on one microcrystal of *Microdictyon* cellulose. The diagram in 5A (circled 1) is of a pure monoclinic crystalline form; the diagram in Figure 5A (circled 2) contains spots corresponding to both the monoclinic and the triclinic forms; the diagram in Figure 5A (circled 3) is of a pure triclinic form. (B) Corresponding indexation. (C) Projection of the reciprocal monoclinic lattice as in Figure 4C. The line marked circled 1 corresponds to the trace of the sectino that is presented in Figure 5A (circled 1). (D) Projection of the reciprocal triclinic lattice as in Figure 3C. The lines marked circled 2 and 3 correspond to the traces of the sections that are presented in Figure 5A (circled 2) and 5A (circled 3). Both components were recorded at 50-nm distances, suggesting that the corresponding microfibril was twisted about its axis.

boundary between the two phases appears to be quite sharp as one goes from a pure monoclinic diagram to a pure triclinic one in about 100 nm.

In order to visualize the crystalline blocks corresponding to each phase in the initial unannealed samples, dark-field electron microscopy was attempted by selecting diffraction spots that are specific of each phase. For instance, the triclinic domains can be revealed by selecting the diffraction spot  $\bar{1}03$  (in the triclinic pattern). In Figure 6 the triclinic crystalline blocks are visualized within a bundle of parallel microfibrils of *Microdictyon*. They consist of a series of white elongated areas having lengths

of several hundred nanometers and widths on the order of 20–30 nm. These blocks, therefore, encompass the whole width of the microfibrils, and this is why an electron diffraction pattern recorded on only 50 nm will yield typical single-crystal diffractograms, in particular, of the triclinic phase. Attempts to visualize the monoclinic crystalline blocks within the unannealed samples were also made by selecting the 002 (in the monoclinic pattern), which is specific to this phase. Unfortunately, this diffraction spot, being rather weak, yields dark-field images of very low contrast, which cannot give any details on the organization of the monoclinic phase in the microfibrils or microcrys-

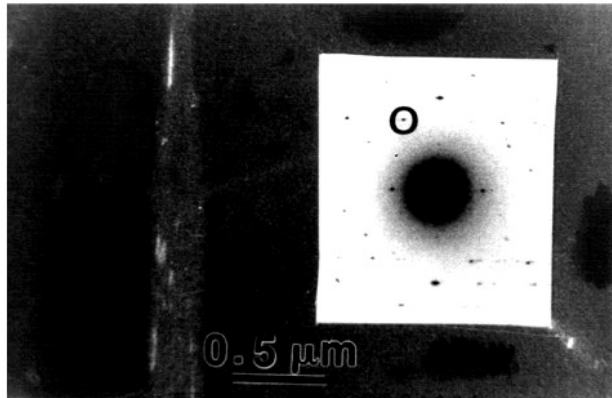


**Figure 6.** Dark-field electron micrograph of a bundle of microfibrils from *Microdictyon*. The picture was made with the use of the  $\bar{1}03$  spot (circled in black), which is specific of the triclinic phase.

tals of *Microdictyon* cellulose.

## Discussion

The diffraction data presented in this study prove that there are two distinct crystalline phases in native *Microdictyon* cellulose: a monoclinic  $P2_1$  phase with two chains per unit cell together with a triclinic  $P1$  phase with one chain per unit cell. The triclinic phase is metastable as it can be converted into the more dense monoclinic phase after annealing in diluted aqueous NaOH<sup>17</sup> or various organic solvents.<sup>22</sup> Thus, the monoclinic phase appears to be the more stable form of these two native celluloses.

Our results with *Microdictyon* cellulose can be extended to other algal celluloses such as those of *Valonia* or *Chetomorpha*. For these samples, an eight-chain unit cell had to be invoked to give a full indexation of their fiber diffraction diagram in terms of a one-chain component.<sup>9,11</sup> The two-phase hypothesis that is presented in this report proposes an alternative that leads also to a full indexation of these fiber diagrams. One of the great advantages of the two phases to describe the crystalline cellulose found in algal cell wall is that these two phases explain quite well the spectral splitting observed in the  $^{13}\text{C}$  CP/MAS NMR spectra of these specimens. According to VanderHart and Atalla, who were the first to reveal and explain this phenomenon,<sup>13,14</sup> *Valonia* cellulose consists of two different phases I $\alpha$  and I $\beta$ , with I $\alpha$  being the major component. There is a majority of the phase I $\alpha$  together with a minor amount of another phase I $\beta$ . Following a preliminary report where the two crystalline phases of cellulose were discussed,<sup>12</sup> we confirm here that the two-chain monoclinic phase of algal cellulose is the I $\beta$  phase found by  $^{13}\text{C}$  CP/MAS NMR, whereas the triclinic phase corresponds to I $\alpha$ . Previously,<sup>12</sup> only fiber diagrams were analyzed, and for this reason, the unit cell of triclinic cellulose could not be given with certainty. The present diffractograms are more informative as they are obtained on individual monocrystalline triclinic blocks of cellulose. In particular, the analysis of these triclinic diagrams indicates that all the reflections of these patterns can be indexed with a one-chain unit cell.

The relative orientation of the triclinic and monoclinic unit cells is shown in Figure 7. The one-chain triclinic cell (bold line) is a single-chain version of the cell proposed by Sarko and Muggli.<sup>3</sup> Being a one-chain cell, it requires all the cellulose chains to be packed in a parallel fashion throughout the triclinic crystalline blocks. Within the triclinic structure, it is cellobiose and not glucose that is the crystallographic-independent repeat. A study of the cell geometry indicates that the cellulose molecules are organized in sheets along the (110) planes where the cel-

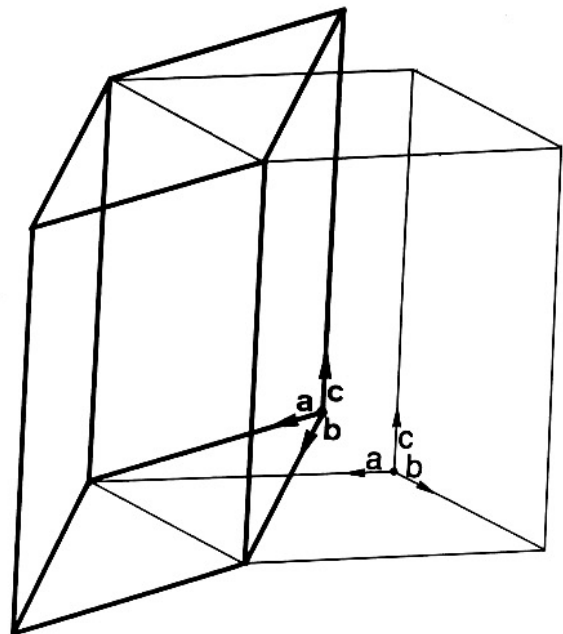


**Figure 7.** Relative orientation of the one-chain triclinic unit cell with respect to the two-chain monoclinic cell.

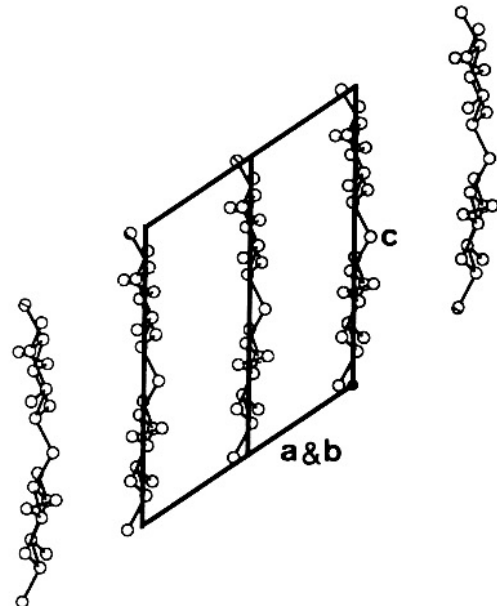


**Figure 8.** Schematic drawing of five cellulose chains viewed parallel to the (110) planes of the one-chain triclinic unit cell. The drawing corresponds to the "parallel up" situation.

lobiose moieties are at the same level along the chain axis. Along the (110) planes, the cellobiose residues follow the slope of the unit cell base, which positions them at  $c/4$  with respect to their neighbors. There are two possibilities for the orientation of the cellobiose residues within the cell: either "up" (with the  $z$  coordinate of O5 being greater than that of C5) or "down" (with the  $z$  coordinate of O5 being smaller than that of C5). In Figure 8 is represented a schematic drawing of the staggering of the cellulose chains along the (110) planes in the triclinic case. This drawing corresponds to the parallel up situation. A similar drawing could also be established in the parallel down case.

Our monoclinic cell (thin line in Figure 7) is the same as those in the literature<sup>2,4-8,12</sup> except for the two parameters  $a$  and  $\gamma$ , which are slightly larger than those quoted for algal cellulose: 0.801 nm vs the 0.78/0.79 nm for  $a$  and an increase of about 1° for  $\gamma$ . These small differences are not due to the use of electrons instead of X-ray to record the diffraction diagrams. In a recent report, Yamamoto

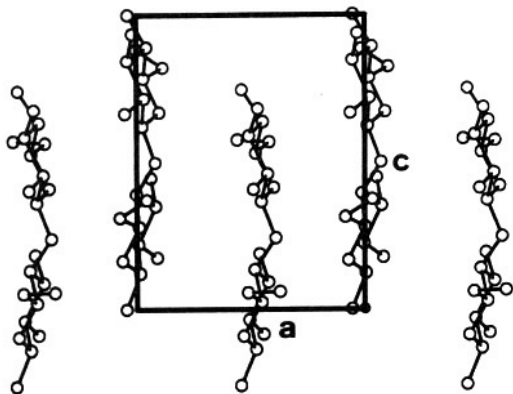


**Figure 9.** Schematic drawing of five cellulose chains viewed along  $b$  of the two-chain monoclinic unit cell. The drawing corresponds to the "parallel up" situation, with the center chain down by  $c/4$  with respect to the corner chains.

et al.<sup>17</sup> have indeed shown by X-ray analysis that the alkaline hydrothermal annealing of *Valonia* cellulose led to small shifts in some of the equatorial reflection of cellulose when a total conversion to cellulose I $\beta$  had taken place. These small shifts account well for the monoclinic cell parameters that are presented here. When celluloses other than algal cellulose are considered, unit cell parameters such as those reported here are sometimes found. The  $a$  parameters for hardwood and bamboo celluloses have been reported to be 0.802 and 0.807 nm, respectively.<sup>23</sup>

The exact position of the cellulose chains in the monoclinic unit cell is more difficult to ascertain as long as the structure refinement is not achieved. Nevertheless, this structure must consist of parallel chains since it is produced, in particular, when the all-parallel triclinic structure is annealed under conditions where the cellulose microfibrillar nature is preserved. In addition, in this monoclinic structure, it is likely that the cellulose chains are positioned on the screw axes of the unit cell and that the center and corner chains are staggered by  $c/4$ . Indeed such chain localization and staggering is consistent with the relative intensities of the meridional diffraction spots as the diffraction spot 004 is much more intense than the 002 (Figure 5). In fact all the two-chain cellulose structures that have been refined so far have localized the cellulose chains in such a mode.<sup>2,4-8</sup> In Figure 9 is presented the staggering of the cellulose chains along the  $b$  axis of the monoclinic structure. This situation corresponds to the "parallel up" situation described in conformity with the convention of French and Howley.<sup>5</sup> Another model, corresponding to the "parallel down" case, could also be drawn, and the choice between the two possibilities cannot be made at this stage. In Figure 9 there is a succession of chains with 0 and  $c/4$  translations. This is quite different from the situation in the triclinic case (Figure 8) where the staggering is always increasing (or decreasing in the case of parallel down situation) along a series 0,  $c/4$ ,  $c/2$ ,  $3c/4$ , etc.

The results presented here need now to be substantiated by a refinement based on diffraction intensity data. For this, one must obtain X-ray diagrams of the pure I $\alpha$  and pure I $\beta$  phases. At present, no pure I $\alpha$  sample has been found, and the only data that are available are the electron diffraction diagrams collected in this study and exemplified

in Figure 3. These diagrams are presently being evaluated for a structure refinement of the I $\alpha$  phase, which should be presented in the near future. For the I $\beta$ , it has been shown<sup>14,24</sup> that tunicate cellulose consisted of highly crystalline material that was entirely of the I $\beta$  phase. The preparation of oriented fibers from this material is one of our goals, as it is the necessary step leading to the recording of informative X-ray fiber diagrams. If this can be achieved with success, the exploitation of these patterns, in combination with the above electron diffractograms, should lead to a reliable structure determination of the pure I $\beta$  phase of cellulose. It is only after the precise determination of both the I $\alpha$  and I $\beta$  structures that one will be able to understand the fine details of the molecular mechanism leading to the solid-state transformation I $\alpha \rightarrow$  I $\beta$ . When comparing the two schematic drawings in Figures 8 and 9, one sees that some cellulose chain slippage or chain rotation is required to achieve this transformation. This implies a substantial rearrangement of the intermolecular hydrogen-bond pattern, which so far has not been described with too much precision for cellulose.

**Acknowledgment.** We thank the late B. Caram for the gift of *Microdictyon tenuius* that was used throughout this study. We are also grateful to A. French and T. Okano for valuable suggestions during the writing of this work.

## References and Notes

- (1) Mark, H.; Meyer, K. H. *Ber. Dtsch. Chem. Ges.* 1928, **61B**, 593.
- (2) Meyer, K. H.; Misch, L. *Helv. Chim. Acta* 1937, **11**, 534.
- (3) Sarko, A.; Muggli, R. *Macromolecules* 1974, **7**, 486.
- (4) Gardner, K. H.; Blackwell, J. *Biopolymers* 1974, **13**, 1975.
- (5) French, A. D.; Howley, P. S. In *Cellulose and Wood, Chemistry and Technology*; Schuerch, C., Ed.; Wiley: New York, 1989; p 169.
- (6) Woodcock, C.; Sarko, A. *Macromolecules* 1980, **13**, 1183.
- (7) Miller, D. P.; Li, A. In *Cellulose and Wood, Chemistry and Technology*; Schuerch, C., Ed.; Wiley: New York, 1989; p 139.
- (8) Millane, R. P.; Narasaiah, T. V. In *Cellulose and Wood, Chemistry and Technology*; Schuerch, C., Ed.; Wiley: New York, 1989; p 39.
- (9) Honjo, G.; Watanabe, M. *Nature* 1958, **181**, 326.
- (10) Fischer, D. G.; Mann, J. J. *J. Polym. Sci.* 1960, **42**, 189.
- (11) Nieduszynski, I. A.; Atkins, E. D. T. *Biochim. Biophys. Acta* 1970, **22**, 109.
- (12) Sugiyama, J.; Okano, T.; Yamamoto, H.; Horii, F. *Macromolecules* 1990, **23**, 3196.
- (13) Atalla, R. H.; VanderHart, D. L. *Science* 1984, **223**, 283.
- (14) VanderHart, D. L.; Atalla, R. H. *Macromolecules* 1984, **17**, 1465.
- (15) VanderHart, D. L.; Atalla, R. H. *The Structure of Cellulose*; ACS Symposium Series 340; American Chemical Society: Washington, DC, 1987; p 88.
- (16) Horii, F.; Yamamoto, H.; Kitamaru, R.; Tanahashi, M.; Higuchi, T. *Macromolecules* 1987, **20**, 2946.
- (17) Yamamoto, H.; Horii, F.; Odani, H. *Macromolecules* 1989, **22**, 4130.
- (18) Sugiyama, J.; Persson, J.; Chanzy, H. *Macromolecules*, in press.
- (19) Riecke, W. D.; Ruska, E. In *Electron Microscopy*; Uyeda, R., Ed.; Maruzen Co., Ltd.: Tokyo, 1966; p 19.
- (20) Thompson, M. N.; Bevis, M. *8th International Congress on EM*; Australian Academy of Science: Canberra, Australia, 1974, p 720.
- (21) Sugiyama, J.; Harada, H.; Fujiyoshi, Y.; Uyeda, N. *Planta* 1985, **166**, 161.
- (22) Debzi, M.; Chanzy, H.; Sugiyama, J.; Tekely, P.; Excoffier, G. submitted for publication in *Macromolecules*.
- (23) Okano, T.; Koyanagi, A. *Biopolymers* 1986, **25**, 851.
- (24) Belton, P. S.; Tanner, S. F.; Cartier, N.; Chanzy, H. *Macromolecules* 1989, **22**, 1615.

**Registry No.** Cellulose, 9004-34-6.